Inorganic Chemistry

Article

pubs.acs.org/IC

Marked Difference in the Electronic Structure of Cyanide-Ligated Ferric Protoglobins and Myoglobin Due to Heme Ruffling

Sabine Van Doorslaer,*[,†] Lesley Tilleman,[‡] Ben Verrept,[†] Filip Desmet,[†] Sara Maurelli,[†,§] Florin Trandafir,[†] Luc Moens,[‡] and Sylvia Dewilde[‡]

[†]Department of Physics and [‡]Department of Biomedical Sciences, University of Antwerp, B-2610 Antwerp, Belgium

[§]Dipartimento di Chimica, Università di Torino and NIS, Nanostructured Interfaces and Surfaces Center, I-10125 Torino, Italy

Supporting Information

ABSTRACT: Electron paramagnetic resonance experiments reveal a significant difference between the principal *g* values (and hence ligand-field parameters) of the ferric cyanide-ligated form of different variants of the protoglobin of *Methanosarcina acetivorans* (*Ma*Pgb) and of horse heart myoglobin (hhMb). The largest principal *g* value of the ferric cyanide-ligated *Ma*Pgb variants is found to be significantly lower than for any of the other globins reported so far. This is at least partially caused by the strong heme distortions as proven by the determination of the hyperfine interaction of the heme nitrogens and mesoprotons. Furthermore, the experiments confirm recent theoretical predictions [Forti, F.; Boechi, L., Bikiel, D., Martí, M.A.; Nardini, M.; Bolognesi, M.; Viappiani, C.; Estrin, D.; Luque, F. J. *J. Phys. Chem. B* **2011**, *115*, 13771−13780] that Phe(G8)145 plays a crucial role in the ligand modulation in *Ma*Pgb. Finally, the influence of the N-terminal 20 amino-acid chain on the heme pocket in these protoglobins is also proven.

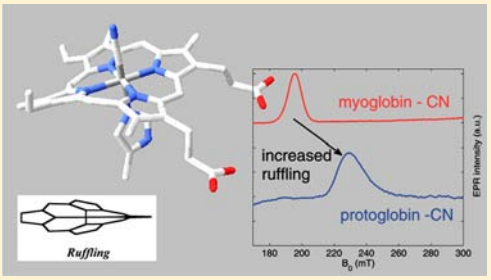

INTRODUCTION

Globins are heme-containing proteins that are found in all kingdoms of life. They exhibit a large variety of biological functions.[1] The most well-documented globins are undoubtedly the mammalian myoglobins (Mbs) and hemoglobins (Hbs).[1] These globins adopt a common 3-over-3 helical sandwich fold, with the low polarity pocket that holds the iron protoporphyrin IX (heme) group. The heme iron is bound to the conserved proximal His residue at position 8 of the F helix (His(F8)), with the sixth (distal) coordination site open for binding to exogenous ligands, like O_2 and NO.

In contrast, far less is known about protoglobins (Pgbs). These are recently discovered single-domain archaeal heme proteins with as yet unknown functions.[2] They have been related to the N-terminal domain of globin-coupled sensors, but they do not simultaneously exist in a single organism.[2−4] At present, nine Pgbs have been identified both in archaea and bacteria,[3,5] but a crystal structure is only available for a number of mutants of the homodimeric protoglobin of *Methanosarcina acetivorans* (*Ma*Pgb).[6,7]

Methanosarcinae are metabolically and physiologically the most versatile methanogens, being the only species endowed with all three known pathways for methanogenesis,[8] which plays a crucial role in the global carbon cycle and global warming. *M. acetivorans* is a strictly anaerobic methanogenic archaeon. Phylogenetic analysis places these ancient organisms at the deepest branching chemoautotrophs on the tree of life.[9,10]

The X-ray structure of the oxygenated ferrous form of *Ma*Pgb* (*Ma*Pgb with a Cys(E20)101→Ser mutation) revealed a number of structural features that are highly unusual for globins: (i) a highly distorted heme completely buried in the protein matrix by a number of protoglobin-specific loops including a 20 amino-acid long N-terminal loop, (ii) a protein fold consisting of nine main helices (Z, A, B, C, E, F, G, H, and H′), and (iii) two apolar tunnels allowing access of exogeneous ligands to the heme center.[6] Although it is at present unclear what specifically causes the heme distortions, the crystal structure reveals different protein-heme interactions, such as residue-pyrrole $\pi-\pi$ interactions, hydrogen bonds, and salt bridges at the propionates and a stabilization of the propionates by a water molecule.[6] The amino-acid residues Tyr(B10)61 and Ile(G11)149 were found to affect the ligand binding to the heme iron and the structural arrangement at the distal side of the heme.[7] Recent molecular dynamics computations predict that the phenylalanine residue at position 8 of the G helix (Phe(G8)145) plays an important role in controlling the ligand accessibility through one of the tunnels.[11] The theoretical data even suggest that *Ma*Pgb may be involved in a ligand-controlled bimolecular chemical process.[11]

In the present work, we compare the cyanide-ligated ferric forms of *Ma*Pgb mutants with the cyanide-ligated ferric form of horse heart myoglobin (hhMb) by means of electron paramagnetic resonance (EPR). The EPR technique allows direct probing of the local environment of the ferric heme center.[12] Several EPR parameters of cyanide-ligated mammalian myoglobins[13−16] have been reported as well as different crystal

Received: April 5, 2012
Published: August 9, 2012

   dx.doi.org/10.1021/ic3007074 | *Inorg. Chem.* 2012, 51, 8834−8841

structures.[17,18] Hence, this molecule forms an ideal system to compare with the cyanide-ligated *Ma*Pgb*. We focus here on three *Ma*Pgb mutants, namely, *Ma*Pgb*, *Ma*Pgb*F(G8)145W, and *Ma*Pgb*-20AA (*Ma*Pgb* lacking the N-terminal 20 amino acids). In the crystal structure of oxygenated ferrous *Ma*Pgb*,[6] the latter N-terminal loop is held next to the heme propionates by different hydrogen bonds (see also Supporting Information, Figure S1). Removal of this loop may influence the heme site. In turn, the Phe(G8)145 amino acid residue is found in one of the aforementioned tunnels at position 8 of helix G close to the heme[6] (Figure 1a). Change of this amino acid may thus influence the heme cavity and the ligand accesibility. The present work focuses on two major questions: (i) Does deletion of the N-terminal 20 amino acids or mutation of Phe(G8)145 induce a change in the EPR parameters (and hence heme pocket region) of cyanide-ligated ferric MaPgb*?, and (ii) How does the electronic structure of cyanide-ligated ferric Mbs and Pgbs compare? For the latter question, pulsed EPR methods are used to extensively study cyanide-ligated hhMb and *Ma*Pgb*F(G8)145W.

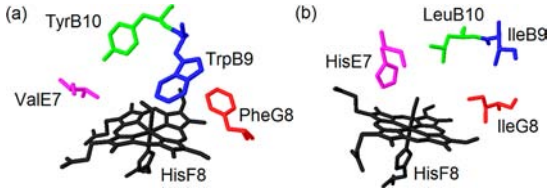

Figure 1. View of the heme site of (a) oxygenated ferrous *Ma*Pgb* (structure from PDB bank (2VEB), 1.3 Å resolution[6]) and (b) cyanide-ligated SwMb (PDB 2JHO, 1.4 Å resolution[17]) highlighting a number of important differences in the amino-acid residues of the heme pocket.

EXPERIMENTAL SECTION

Recombinant Expression of *Ma*Pgb* and Mutants. Mutations were introduced in *Ma*Pgb using the QuickChange site-directed mutagenesis method (Stratagene), as described previously.[19] The mutant bearing the C(E20)101S substitution is annotated as *Ma*Pgb*. To narrow tunnel 1, the *Ma*Pgb* F(G8)145W mutant was designed, where phenylalanine is substituted by the bulkier amino acid tryptophan. *Ma*Pgb*-20AA is the mutant of *Ma*Pgb* that lacks the N-terminal loop. The recombinant proteins were expressed in *Escherichia coli* Bl21(DE_3)pLysS cells and collected as described previously.[19] Alternatively, the cells were resuspended in 50 mM Tris–HCl pH 8.0, 5 mM EDTA, 0.5 mM dithiothreitol, and 1 mM phenylmethylsulfonyl fluoride.

Purification of *Ma*Pgb* and Mutants. The cells were exposed to three freeze–thaw steps and sonicated until completely lysed. Inclusion bodies were washed twice with 50 mM Tris–HCl pH 8.0, 5 mM EDTA, and 2% sodium deoxycholate, washed once with pure water and solubilized by incubation in 100 mM Tris-NaOH pH 12.0 and 2 M urea. After an incubation period of 30 min at room temperature and centrifugation at 10,700 *g* for 20 min at 4 °C, *Ma*Pgb* was refolded by adding a 1.5 M excess of hemin (7.6 mM in 10 mM NaOH). After an incubation period of another 10 min at room temperature, the pH was adjusted to 8.5 with HCl. The solution was then diluted into 5 volumes of distilled water and finally dialyzed at 4 °C against gel filtration buffer (50 mM Tris-HCl pH 8.5, 150 mM NaCl, and 0.5 mM EDTA). Final purification was performed by gel filtration using a Superdex G75 column equilibrated in this buffer.

Preparation of the Cyanide-Ligated Ferric Forms of *Ma*Pgb* and hhMb. Ferric horse heart myoglobin (hhMb) was purchased from Sigma-Aldrich as lyophilized powder. This powder was then dissolved in a 50 mM Tris–HCl buffer at pH 8.0. The ferric cyanide-ligated forms of *Ma*Pgb*, its site-directed mutants, and hhMb were prepared by adding a 40 times excess of KCN (Sigma-Aldrich) to the as expressed ferric proteins. No significant change to the pH was detected. For low-temperature EPR measurements, 20 wt % of the cryoprotectant glycerol was added to the solution. The final concentrations were 2 mM for hhMbCN and 0.3–0.6 mM for the cyanide-ligated variants of *Ma*Pgb*.

EPR Spectroscopy. X-band continuous-wave (CW) EPR measurements were performed on a Bruker ESP 300E spectrometer (microwave frequency 9.44 GHz) equipped with a liquid Helium cryostat (Oxford Inc.). EPR spectra were obtained with a modulation frequency of 100 kHz. The modulation amplitude and microwave power are given in the figure captions. The EasySpin program was utilized to simulate the CW-EPR spectra.[20]

X-band pulsed EPR experiments were performed on a Bruker Elexsys instrument equipped with Helium cryostat (Oxford Inc.). The measurements were done at 4 K.

Electron spin echo (ESE)-detected EPR experiments were performed using the $\pi/2$-τ-π-τ-echo sequence with $t_{\pi/2}$ = 16 ns, t_π = 32 ns; τ was varied in steps of 8 ns.

Hyperfine sublevel correlation (HYSCORE) experiments[21] were done with the pulse sequence: $\pi/2$-τ-$\pi/2$-t_1-π-t_2-$\pi/2$-τ-echo, with $t_{\pi/2}$ = 16 ns and t_π = 32 ns; t_1 and t_2 were varied in steps of 16 ns (matrix dimension [350 × 350]). Alternatively, the SMART (single matched resonance transfers)-HYSCORE sequence,[22] HTA-t_1-π-t_2-HTA-τ-π-τ-echo, was used with a π pulse of 16 ns and a τ value of 96 ns. The power and length of the high-turning angle (HTA) pulses was adjusted using a matched three-pulse ESEEM experiment.[23] The optimized parameters are given in the figure captions. A four-step phase cycle was performed in all cases to remove the unwanted echoes. The HYSCORE traces were baseline corrected using a third-order polynomial, apodized with a Hamming window, and zero-filled. After Fourier transformation the absolute-value spectra were computed. All spectra were simulated using the EasySpin program.[20] In some cases, the experimental HYSCORE spectra were symmetrized to improve signal-to-noise. This was only done for those cases where this procedure induced no new signals.

^{1}H-Mims ENDOR experiments[24] were performed using the microwave pulse sequence $\pi/2$-τ-$\pi/2$-T-$\pi/2$-τ-echo with $t_{\pi/2}$ = 16 ns and a π rf pulse of 8 μs during the time T. Spectra were recorded at 20 τ values ranging from 96 to 248 ns and added together to avoid blindspots. An ENI A-300 rf amplifier was used. Davies ENDOR experiments[25] were performed using the microwave pulse sequence π-T-$\pi/2$-τ-π-τ-echo, with $t_{\pi/2}(t_\pi)$ = 48(96) ns (hhMbCN) or $t_{\pi/2}(t_\pi)$ = 16(32) ns (*Ma*Pgb*F(G8)145WCN). Different microwave pulse lengths were tested and only the ones that gave the best final result are reported here. During time T, an rf pulse of length 6 μs (hhMbCN) or 8 μs (*Ma*Pgb*F145WCN) was applied. The spectra were collected in stochastic mode.

RESULTS

X-Band Continuous-Wave (CW) EPR Experiments. Figure 2 shows the CW-EPR spectra of the cyanide-ligated ferric forms of (a) hhMb, (b) *Ma*Pgb*, (c) *Ma*Pgb*F(G8)-145W, and (d) *Ma*Pgb*-20AA recorded at 5 K. The spectra are typical for low-spin ferric heme centers. The high-field feature could not be resolved in the EPR spectra; an upper value for the g_x value was determined from the highest field value at which a significant spin echo and echo modulation could be detected (Table 1; Supporting Information, section S2). The principal g values of cyanide-ligated ferric hhMb are very similar to those found for cyanide-bound swMb[13] and present the typical high maximal g value (g_{max} > 3.3) observed for most CN^- ligated globins.[12,26–29]

In contrast, cyanide ligation leads, for the three *Ma*Pgb mutants studied in this work, to g_{max} values that are unusually low compared to other globins (Table 1, Figure 2b–d). Furthermore, a clear difference is observed in the g values of the

dx.doi.org/10.1021/ic3007074 | Inorg. Chem. 2012, 51, 8834–8841

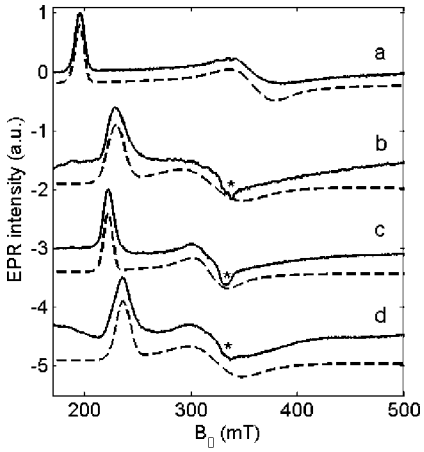

Figure 2. X-band CW-EPR spectra of frozen solutions of the cyanide-ligated ferric form of (a) hhMb, (b) *Ma*Pgb*, (c) *Ma*Pgb*F(G8)-145W, and (d) *Ma*Pgb*-20AA. All spectra were recorded at 5 K, with a modulation amplitude of 0.5 mT, 0.25 mW microwave power, and varying number of scans to match the difference in concentration. The spectra are rescaled to a microwave frequency of 9.44 GHz and normalized to allow comparison. The asterisk indicates a small background feature due to Cu(II). Solid line: experiment, dashed line: simulation.

Table 1. Principal *g* Values Obtained from the Simulation of the X-Band EPR Spectra of Frozen Solutions of the Cyanide-Ligated Ferric Globins Studied in This Work Compared to Related Systems Reported in Literature

CN^- ligated ferric form of	g_x	g_y	g_z	ref.
hhMb	≤0.92	1.86 (±0.02)	3.420 (±0.005)	this work
*Ma*Pgb*	≤0.99	2.08 (±0.02)	2.91 (±0.01)	this work
*Ma*Pgb*F(G8)145W	≤0.96	2.10 (±0.02)	3.015 (±0.005)	this work
*Ma*Pgb*-20AA	≤0.99	2.06 (±0.02)	2.83 (±0.01)	this work
SwMb[a]	0.93	1.871	3.442	13, 15
*Dm*Hb[a]	n.d.[b]	n.d.[b]	3.43	26
soybean legHb[a]	1.0	1.97	3.35	27
barley Hb	n.d.[b]	n.d.[b]	3.32	28
horseradish peroxidase	1.2	2.1	3.05	29
myeloperoxidase	1.66	2.25	2.83	29
cytochrome P450	1.80	2.28	2.63	30

[a]SwMb = Sperm whale myoglobin; DmHb = Hemoglobin (Hb) of *Drosophila melanogaster*; legHb = leghemoglobin. [b]n.d. = not determined.

three *Ma*Pgb* variants. The largest change is observed when the Phe(G8)145 residue is replaced by Trp. This shows that this residue directly affects the distal heme side. The effect of the removal of the N-terminal loop is less pronounced, but still significant. This indicates that the interaction of this loop with the heme ligand observed in the crystal structure[6] of *Ma*Pgb*O_2 (Supporting Information, Figure S1) is not due to crystal packing effects, but holds in solution.

Pulsed EPR Experiments. All currently available crystal structures of *Ma*Pgb* forms and related mutants show a strong distortion of the heme group[6,7] (Figure 1; Supporting Information, Figure S3). Molecular dynamics computations suggest that in-plane heme distortions may be exploited by certain classes of heme proteins, such as Pgbs, to modulate the ligand affinity.[31] Indeed, heme flattening was found to increase the proximal bond strength in the oxy ferrous heme center of the H-NOX domain of *Thermoanaerobacter tengcongensis*.[32] If the heme distortion is also present in the ferric cyanide-ligated *Ma*Pgb* variants studied here, we expect a significant difference between the hyperfine interactions of the heme nitrogens of these variants and those of ferric hhMbCN. Indeed, ruffling will affect the overlap between the Fe and heme orbitals and thus influence the spin density distribution. Furthermore, depending on the heme distortion, the heme nitrogens may become more magnetically inequivalent. Therefore, we compare the ^{14}N HYSCORE data of cyanide-ligated ferric hhMbCN and *Ma*Pgb*F(G8)145WCN. The latter protein was chosen from the set of three proteins because it gave the best protein yield and most intense electron spin echo, allowing for the acquisition of different pulsed EPR experiments within reasonable time frames. Nevertheless, several hours were needed to record a single HYSCORE or ENDOR spectrum in the *Ma*Pgb*F(G8)145WCN case at field settings corresponding with the highest echo intensity (near $g = g_{max}$). At higher fields, the HYSCORE data were of insufficient quality to be analyzed.

Figure 3a shows the standard ^{14}N HYSCORE spectrum of ferric hhMbCN recorded at the single-crystal-like observer position corresponding to $g = g_{max}(= g_z)$. Figure 3b depicts the corresponding standard ^{14}N HYSCORE spectrum for ferric *Ma*Pgb*F(G8)145WCN. It is obvious that the spectra differ significantly.

Earlier EPR and NMR studies revealed that the g_z axis of cyanometmyoglobins lies close to the normal of the heme plane (deviations <15°).[13,33,34] Hyperfine spectroscopy experiments performed at the observer position corresponding to $g = g_z$ will thus return the hyperfine (A_{zz}) and nuclear quadrupole (P_{zz}) values agreeing with this direction in space. For a relatively flat heme, as is the case for cyanometmyoglobins, we expect no or a very small difference in the A_{zz} (P_{zz}) values of the heme nitrogens as is schematically shown in the cartoon in Figure 4a. Although previous CW-ENDOR experiments on ferric swMbCN could not be unambiguously analyzed, the difference between the A_{zz} values of the heme nitrogens was indeed estimated to be very small (between 0 and 0.52 MHz).[14]

In the HYSCORE spectrum of ferric hhMbCN (Figure 3a), the cross peak connecting the double-quantum (DQ) frequencies of the heme nitrogens is found to be very narrow, reminiscent of a very small spread in the A_{zz} and P_{zz} values. The spectral features due to the interactions with the heme nitrogens could be enhanced using matched pulses (Figure 3c). The fact that in the latter spectrum cross peaks involving twice the DQ frequencies can be observed, implies that the cross peaks marked $(-\nu_{DQ}^{\beta},\nu_{DQ}^{\alpha})$ agree with at least two magnetically nearly equivalent nuclei. These can only be the heme nitrogens. The ^{14}N contributions in the HYSCORE spectrum of Figure 3c could be simulated assuming four ^{14}N nuclei with pairwise equivalent parameters: $|A_{zz,1-2}| = 5.8(\pm0.1)$ MHz, $|P_{zz,1-2}| = 0.40(\pm0.05)$ MHz, and $|A_{zz,3-4}| = 6.1(\pm0.1)$ MHz, $|P_{zz,3-4}| = 0.40(\pm0.05)$ MHz (Figure 5a). The overlay of the spectra is shown in the Supporting Information to allow evaluation of the quality of the simulation (Supporting Information, Figure S5). When a larger spread in the heme nitrogen hyperfine values was taken, the simulation was no longer acceptable.

dx.doi.org/10.1021/ic3007074 | *Inorg. Chem.* 2012, 51, 8834−8841

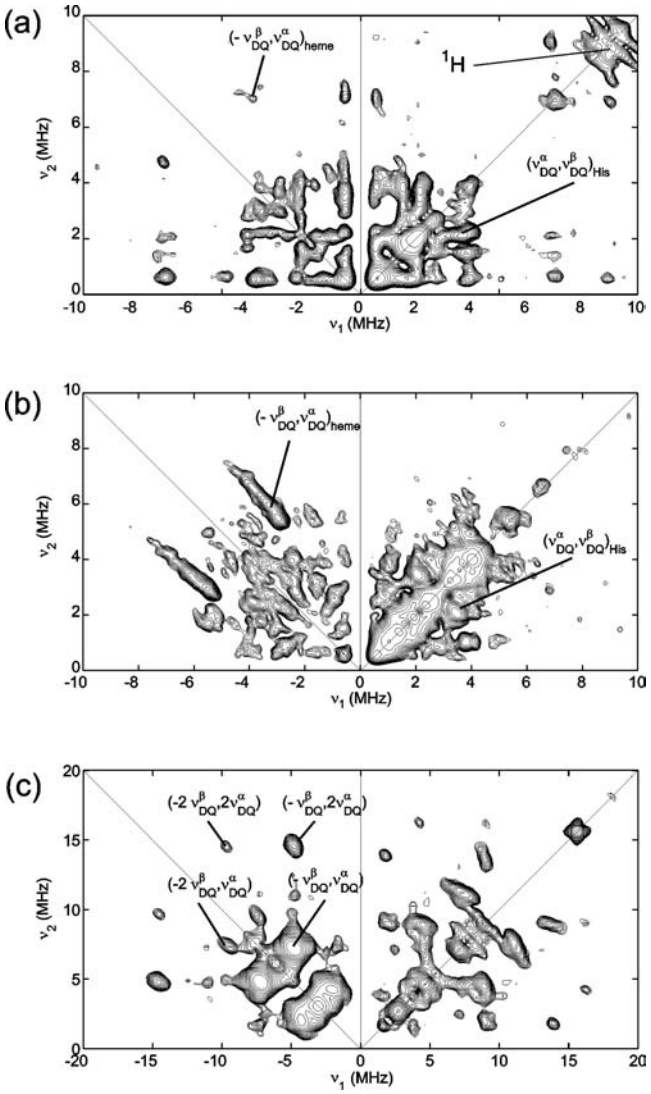

Figure 3. (a) Experimental HYSCORE spectrum of a frozen solution of ferric hhMbCN taken at 4 K at an observer position agreeing with $g = g_z$ (B_0 = 212.5 mT). The spectrum is the sum of the spectra taken with τ values 120 and 176 ns. (b) Experimental HYSCORE spectrum of a frozen solution of ferric *Ma*Pgb*F(G8)145WCN taken at 4 K at an observer position agreeing with $g = g_z$ (B_0 = 247.0 mT). The spectrum is the sum of the spectra taken with τ values 88, 96, 104, 120, 176, and 284 ns. (c) SMART HYSCORE spectrum of a frozen solution of ferric hhMbCN taken at 4 K at an observer position agreeing with $g = g_z$ (B_0 = 212.5 mT). The length of the HTA pulses is 32 ns, ν_1 = 15.625 MHz.

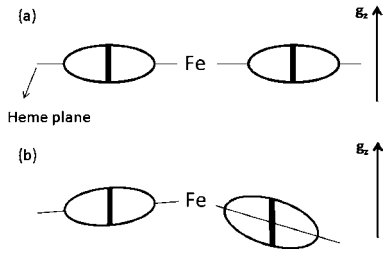

Figure 4. Cartoon explaining the different response expected for a hyperfine spectroscopy experiment performed at an observer position near $g = g_z$ for a ferric heme system with (a) flat heme and (b) strongly distorted heme. The picture is similarly valid for the hyperfine and quadrupole interactions. The ellipses present the hyperfine (or quadrupole) tensors, the thick black line the observed hyperfine (or quadrupole) values. In case (a), the hyperfine (quadrupole) tensors are expected to be very similar and the spectral response will be quasi the same for all heme nitrogens, in case (b) each heme will give a different response because of the different orientation and magnitude of the hyperfine (quadrupole) tensors.

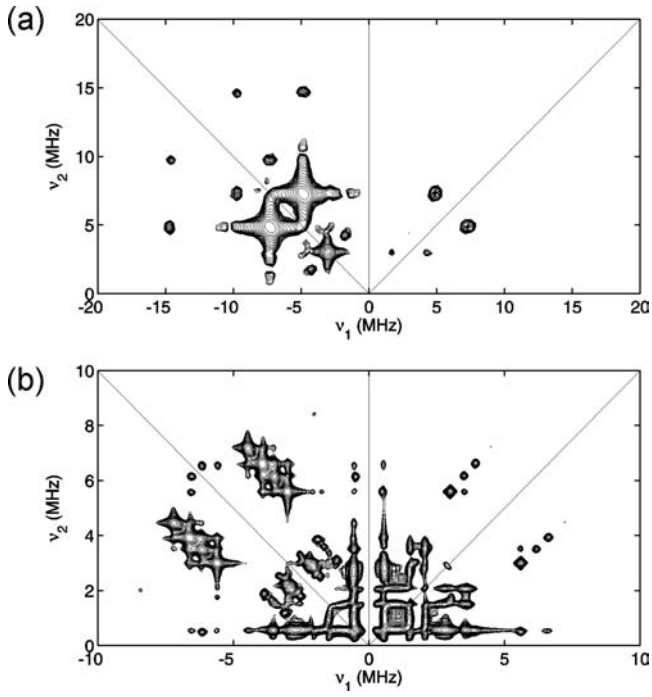

Figure 5. Simulated HYSCORE spectra of (a) experimental SMART HYSCORE spectrum in Figure 3c and of (b) experimental HYSCORE spectrum in Figure 3b. The simulation parameters are given in the text.

The majority of the cross peaks in the (+,+) quadrant of the SMART HYSCORE spectrum stem from the proton nuclear frequencies and combination frequencies between ^{14}N and ^1H nuclear frequencies as demonstrated in the Supporting Information, Figure S6.

In the standard HYSCORE spectrum in Figure 3a, the DQ cross-peaks of the iron-bound histidine nitrogen are also indicated. The comparison of the HYSCORE spectra of ferric hhMbC^{14}N and hhMbC^{15}N confirms that these signals do not stem from the cyanide nitrogen (Supporting Information, Figure S7). Previous ^{14}N three-pulse experiments on ferric hhMbCN revealed for the His nitrogen: $|A_{zz}| \approx 1.5$ MHz, $|P_{zz}| \approx 1.25$ MHz.[16] Reasonable fits of the spectrum in Figure 3a could indeed be obtained when assuming the earlier mentioned heme nitrogen parameters together with a contribution for a histidine nitrogen ($|A_{zz}| \approx 1.7(\pm 0.1)$ MHz, $|P_{zz}| \approx 1.15(\pm 0.10)$ MHz) (Supporting Information, Figure S8).

In the case of ferric *Ma*Pgb*F(G8)145WCN, the HYSCORE cross peaks connecting the DQ nuclear frequencies of the heme nitrogens are elongated ridges instead of narrow peaks (Figure 3b). This indicates a strong inequivalence of the ^{14}N hyperfine and/or quadrupole tensors as is expected in the case of strong heme distortions (Figure 4b). In contrast to the hhMbCN case, no suitable matching condition to enhance these signals could be found. The extension of the heme ^{14}N DQ ridge in Figure 3b could only be simulated when four inequivalent heme nitrogens were assumed with $|A_{zz}|$ values varying between 3.9 and 5.6 MHz (±0.1 MHz). The cross peaks stemming from the DQ ^{14}N frequencies of the iron-bound histidine nitrogen are

dx.doi.org/10.1021/ic3007074 | *Inorg. Chem.* 2012, 51, 8834–8841

Table 2. ^{14}N Hyperfine (A_{zz}) and Nuclear Quadrupole (P_{zz}) Values Determined at an Observer Position Corresponding to $g = g_z$ for the Cyanide-Ligated Ferric Globins Studied in This Work Compared to Related Systems Reported in Literature

	$\lvert A_{zz}\rvert$/MHz	$\lvert P_{zz}\rvert$/MHz	method	ref.
		Heme Nitrogens		
hhMbCN	5.8/6.1	0.4	HYSCORE	this work
*Ma*Pgb*F(G8)145WCN	3.9−5.6	0.2	HYSCORE	this work
SwMbCN[a,b]	7.15	0.15	CW ENDOR	14
	5.84/6.36	0.6/0.58		
Cyt P450 CN[a]	5.2/5.9	0.27	CW ENDOR	30
Aquomet hhMb	7.1/7.7	0.33/0.23	HYSCORE ENDOR	35
Ferric human neuroglobin	5.7	0.52	HYSCORE	36
		Iron-Binding Nitrogen of Proximal His		
hhMbCN	1.7	1.15	HYSCORE	this work
*Ma*Pgb*F(G8)145WCN	1.5	1.2	HYSCORE	this work
SwMbCN	1.5	1.25	3-pulse ESEEM	16
Aquomet hhMb	11.5	1.28	HYSCORE ENDOR	35
Ferric human neuroglobin	4.9	0.8	HYSCORE	36

[a]SwMb = Sperm whale myoglobin; Cyt P450 = cytochrome P450. [b]There is an ambiguity in the spectral interpretation; two possible interpretations were reported for this case.

very similar to those found for the hhMbCN case (compare the signals in the (+,+) quadrants of Figures 3a and 3b). Figure 5b shows a simulation assuming the contributions of four heme nitrogens with $|A_{zz,1}| = 5.6$ MHz, $|A_{zz,2}| = 5.0$ MHz, $|A_{zz,3}| = 4.5$ MHz and $|A_{zz,4}| = 3.9$ MHz and $|P_{zz,n}| = 0.2$ MHz ($n = 1-4$) and one histidine nitrogen with $|A_{zz}| = 1.5$ MHz and $|P_{zz}| = 1.2$ MHz. The overlay of the spectra is shown in the Supporting Information, Figure S9. The agreement is not perfect, mainly because we neglect here the effect of dynamics in solution and the consequent heterogeneity of the heme conformations in the frozen solution. This heterogeneity will lead to an elongation of the individual peaks, giving rise to DQ ridges instead of the collection of DQ peaks in Figure 5b. Nevertheless, the simulation proves that indeed several magnetically inequivalent nitrogens need to be taken into account. This is not so surprising if one compares the tilting of the pyrrole rings in MaPgb*O_2 with those in swMbCN (Supporting Information, Figure S4).

The simulation results are summarized in Table 2 and compared to other known heme systems.

Figure 6 shows the comparison between the X-band Davies ^{1}H ENDOR spectra of ferric hhMbCN and MaPgb*F(G8)-145WCN taken at the observer position corresponding with $g = g_z$. The corresponding ^{1}H Mims ENDOR spectra are shown in the Supporting Information, Figure S10. In earlier work, Mulks et al. analyzed the ^{1}H ENDOR spectra of cyanide-ligated swMb.[14] In addition to a central feature centered around the proton Larmor frequency, ν_H, they observed broad, outlying resonances split by ∼4 MHz that could be assigned to the nearby C−H protons of the proximal histidine. Similar weak broad shoulders are also visible in both Davies ENDOR spectra depicted in Figure 6 (dashed lines), which is not unexpected since the heme iron is linked to the protein backbone via the proximal His(F8) in both the myoglobin and protoglobin cases.

By comparing with protoheme cyanide, Mulks et al. could ascribe the outer proton signals of the central feature of the ENDOR spectrum of cyanide-ligated myoglobin (1.75 MHz splitting, indicated with dashed-dotted line in Figure 6) to either the proton on the δ nitrogen of the proximal His or a proton hydrogen bonded to the cyanide.[14,37] Furthermore, a coupling of 1.2 MHz was assigned to the meso protons.

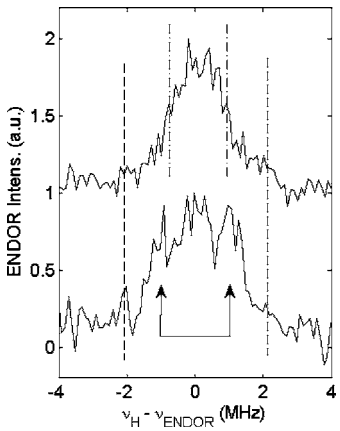

Figure 6. Experimental ^{1}H Davies ENDOR spectra of ferric hhMbCN (top) and ferric *Ma*Pgb*F(G8)145WCN (bottom) taken at an observer position corresponding to $g = g_z$. The explanation of the dashed and dashed-dotted lines and the arrows is given in the main text.

It is clear from Figure 6 that the central proton ENDOR feature is broader in the case of *Ma*Pgb*F(G8)145WCN. Signals with a clear splitting of 2 MHz are observable (arrows in Figure 6). These signals are unlikely to stem from the proton on the δ nitrogen of the proximal His, since hhMbCN and *Ma*Pgb*F(G8)145WCN have essentially the same ^{14}N hyperfine value of the iron-bond imidazole nitrogen (Table 2) and similar C−H proton couplings of the proximal His (Figure 6, dashed lines). In fact, a decrease in the g tensor principal values will also induce a reduction in the dipolar contribution to the proton hyperfine value for the same distance between the δ-N proton and the Fe atom (distance of 5.1 Å leads to $2T = 2.04$ MHz for the MbCN case and 1.8 MHz for the PgbCN case, with $2T$ the maximal value of the point-dipolar contribution, which is approximately found along the g_z direction). If the 1.75 MHz hyperfine splitting in hhMbCN stems from the δ-N proton, this means that the isotropic hyperfine contribution should be either −0.3 MHz or −3.8 MHz. The latter is too large in comparison with the negligible spin density on the δ-N nucleus and with the typical isotropic hyperfine values of around −1 MHz for the C−H protons.[36] Since neither O_2 nor

dx.doi.org/10.1021/ic3007074 | Inorg. Chem. 2012, 51, 8834−8841

H_2O are stabilized by any hydrogen bonds in *Ma*Pgb*O_2 and *Ma*Pgb*Y(B10)61W(H_2O),[6,7,11] it is also very improbable that the 2 MHz proton coupling would arise from a cyanide-stabilizing hydrogen. The meso protons are therefore the most likely candidates, given the large differences between the heme nitrogen hyperfine values of both systems.

DISCUSSION

The ***g*** tensors of low-spin ferric heme centers directly reflect the electronic configuration. In an (over)simplified picture, low-spin ferric porphyrinate systems with maximum g values <2.6 have an electron configuration $(d_{xz},d_{yz})^4(d_{xy})^1$, whereas all other (rhombic) ***g*** tensors of these systems are ascribed to a $(d_{xy})^2(d_{xz},d_{yz})^3$ ground state, which is the most common case.[12] The ***g*** tensors of all the ferric cyanide-ligated globins, including the *Ma*Pgb variants, fall within the latter class (Table 1). Nevertheless, the small g_{max} values of the cyanide-ligated *Ma*Pgb* variants studied in this work are unprecedented when compared with other cyanide-ligated globins. Low ***g*** anisotropy has been reported for cyanide-ligated cytochrome P450 (Table 1),[30] but, other than in the protoglobin case, this can be fully ascribed to the proximal thiolate coordination. The principal g values of the cyanide-ligated *Ma*Pgb* variants are similar to those observed for cyanide-ligated peroxidases (Table 1).[29] In the peroxidase case, the low g_{max} value is induced by the imidazolate character of the proximal His. However, since the hyperfine and nuclear quadrupole values of the iron-binding nitrogen and the His C−H proton coupling in ferric *Ma*Pgb*F(G8)145WCN are the same as those found for hhMbCN (Table 2 and Figure 5), it seems to be unlikely that the proximal His is an imidazolate. Indeed, the hyperfine couplings of the His nitrogen are very sensitive to the overall electronic structure and would clearly reflect the change in the imidazole nature (Table 2).

The unusually low g_{max} value in ferric *Ma*Pgb*F(G8)-145WCN is paralleled with a strong magnetic inequivalence of the heme nitrogens, indicative of strong heme distortions (Figure 3c, Table 2). Strong heme ruffling was indeed found by X-ray diffraction for different oxy-ferrous and ferric *Ma*Pgb variants.[6,7] Interestingly, recent work on cytochrome c_{552} and c_{551} variants showed a modulation of the ligand-field parameters (and thus g values) induced by heme ruffling.[38] The cytochrome c_{552} variants with significant heme ruffling exhibited a lower g_{max} value, and the change of the ligand-field parameters was ascribed to an increase of the energy of the d_{xy} orbital relative to the d_{yz} and d_{xz} orbitals. Moreover, previous work on synthetic ferric (di)cyano and di-isocyano porphyrin systems[39−42] has shown that the principal g values of such systems can vary from the classic "high g_{max} value" case to species exhibiting axial ***g*** tensors with low g_{max} (e.g., ***g*** = [2.42 2.42 1.74][39]). This change from the common $(d_{xy})^2(d_{xz},d_{yz})^3$ configuration to a $(d_{xz},d_{yz})^4(d_{xy})^1$ configuration (g_{max}< 2.6) has also been observed for other axial ligands than cyanide.[40,43] Nakamura and co-workers found that several factors affect this change: the strength of the axial ligands, hydrogen bonding to the cyanide, porphyrin distortions, and substituents on the meso position of the porphyrin ligand.[39,42] Of special interest is the observation that the ferric dicyano porphyrin species that are characterized by an axial ***g*** tensor exhibit strong ruffling of the porphyrin ligand.[39] It is worth mentioning that cyanide-ligated peroxidases, exhibiting g values similar to the cyanide-ligated *Ma*Pgb* variants, have nonplanar hemes, although the hemes are saddled rather than ruffled.

In principle, one can use the principal g values to determine the ligand-field parameters.[12,34,44−47] However, when the ***g*** tensors are obtained from CW-EPR measurements in frozen solution, one cannot link the principal g values to any of the molecular axes. This information can only be obtained from single-crystal EPR work[13] or, in some cases, from pulsed EPR experiments.[48,49] As pointed out by McGarvey,[47] many misinterpretations of the ***g*** tensors of strong field d^5 systems originate from this failure to assign the axes in addition to the fact that the sign of the g values cannot be determined experimentally. Moreover, in the case of the cyanide-ligated *Ma*Pgb* variants, the experimental uncertainty on the g_x value (Table 2) makes an evaluation of the ligand-field parameters very inaccurate (see Supporting Information). We will therefore not attempt such an analysis. Nevertheless, a number of conclusions can already be drawn from inspection of the ***g*** tensor data.

First, while for a fairly pure $(d_{xy})^2(d_{xz},d_{yz})^3$ state the following equation seems to hold[12]

$$g_x^2 + g_y^2 + g_z^2 = 16 \quad (1)$$

this sum is found to be significantly lower than 16 in the case of a $(d_{xz},d_{yz})^4(d_{xy})^1$ ground state or when covalency effects and mixing of excited states due to low symmetry contributions to the crystal field need to be considered.[12,45] Interestingly, the sum of the squares of the principal g values is lower than 16 for all cyanide-ligated *Ma*Pgb variants (*Ma*Pgb*CN: ≤13.8; *Ma*Pgb*F(G8)145WCN: ≤14.4; *Ma*Pgb*-20AACN: ≤13.2), while it equals approximately 16 for the cyanide-ligated Mb cases. The upper limit for g_x in the *Ma*Pgb* variants indeed implies a reduction of the spin−orbit mixing due to low symmetry contributions (see Supporting Information).

The single-crystal EPR analysis of ferric swMbCN revealed that the largest principal g value is along the heme normal,[13] in line with its $(d_{xy})^2(d_{xz},d_{yz})^3$ ground state. The large similarity between the hyperfine values found for the magnetic nuclei of the proximal His of hhMbCN and *Ma*Pgb*F(G8)145WCN at the $g = g_{max}$ observer position (Table 2) indicates that also for the latter protein the maximal g is pointing more or less along the Fe-CN bond. Nevertheless, the difference between the g_z and g_y values has significantly decreased in the *Ma*Pgb* variant case compared to the hhMbCN case (Table 1). This may point to an increased d_{xy} character of the molecular orbital containing the unpaired electron.[38,50] In this respect, it is important to examine more carefully the pulsed EPR results of *Ma*Pgb*F-(G8)145WCN. The $|A_{zz}|$ hyperfine values of heme ^{14}N nuclei are not only very different among each other, but even more interestingly, at least one has a hyperfine value as low as 3.9 MHz. If we compare this with known Fe(III) heme systems that are considered to have a "pure" $(d_{xy})^2(d_{xz},d_{yz})^3$ ground state, all reported $|A_{zz}|$ values of the heme nitrogens are in the order of 5.4−6.1 MHz (Table 2).[14,26,30,51−53] This is found independent of the type of the axial ligands (His, Cys, imidazole, CN^-) and independent of the corresponding g_z values, and hence the ligand-field parameters. In contrast, Astashkin et al.[48] observed hyperfine values for the pyrrole nitrogens of 3.3(±0.5) MHz for bis(phenyl isocyanide) complexes of iron(III) porphyrins exhibiting the $(d_{xz},d_{yz})^4(d_{xy})^1$ ground state. Furthermore, Astashkin et al.[48] found relatively large ^1H hyperfine values for the meso-protons (splitting of 4 to 6 MHz) in contrast to the small splitting (∼1.2 MHz) observed for the meso protons in swMbCN[14]. As shown in Figure 6

dx.doi.org/10.1021/ic3007074 | Inorg. Chem. 2012, 51, 8834−8841

(arrows), the heme ^{1}H couplings of ferric *Ma*Pgb*F145WCN seem to be somewhat larger than those of hhMbCN. This agrees with previous analyses that suggested that the twisting of the pyrrole rings in ruffled hemes tilts the p_z orbitals of the heme nitrogens such that there is a small projection in the *xy* plane leading to a small but significant overlap between the π orbitals of the heme and the d_{xy} orbital. This will influence the spin density on the meso protons.[54]

Heme ruffling is not the only factor known to modulate the ligand-field parameters; other factors, such as the stabilization of the cyanide ligand and orientation of the His(F8) residue versus the heme plane will affect the *g* tensor.[12,55] Part of the ruffling in nitrophorins and cytochromes *c* arises from the fact that the imidazole plane of the proximal histidine is oriented along the meso axes of the heme rather than along the $N_{pyrrole}$−Fe−$N_{pyrrole}$ axis.[55] Although no crystal structure is available for cyanide-ligated protoglobins, all structures of ferrous and ferric protoglobins show the His(F8) imidazole to be approximately along the latter axis (deviations of 8−19°).[6,7] This suggests that the orientation of the His(F8) does not play a dominant role in the ruffling of the *Ma*Pgb variants. In the *Ma*Pgb case, a Val residue is found at position E7 (Figure 1a). This contrasts the presence of the His(E7) residue in all mammalian myoglobins and hemoglobins (Figure 1b), known to stabilize exogenous ligands, such as cyanide.

All the above findings indicate that the electronic structure of the heme site in the *Ma*Pgb* variants differs from the one of the MbCN case. Although the *Ma*Pgb*CN variants can still be classified as belonging to the $(d_{xy})^2(d_{xz},d_{yz})^3$ class, the decreased *g* anisotropy and the altered spin density distribution in the heme plane suggest a larger relative contribution of the d_{xy} orbital in the molecular orbital containing the unpaired electron. Note that the EPR experiments are performed at low temperature and that the electron configuration of the cyanide-ligated *Ma*Pgb* variants may alter to a clear-cut case of $(d_{xz},d_{yz})^4(d_{xy})^1$ at room temperature, as is the case for the nitrophorins. Future NMR studies may help to elucidate this.

The strong heme ruffling, which is observed by X-ray diffraction for different Fe(II) and Fe(III) forms of *Ma*Pgb* variants,[6,7] undoubtedly plays an important role in the observed difference between the protoglobin and the myoglobin cases. Although it is as yet unclear how this ruffled heme is induced, comparison with the nitrophorin case suggests that bulky amino acid residues, perpendicularly oriented to the heme plane may selectively push the pyrrole rings out of the porphyrin ring.[56,57] The functional effects of heme ruffling are still highly debated. In cytochrome c_{552} variants, enhanced heme ruffling and His-Fe(III) bond strength seem to be correlated with decreasing reduction potential.[38] Conflicting data on a possible relation between heme ruffling and His-Fe(III) bond strength have been reported.[50,58] Our current results do not show major changes between the hyperfine data of the ^{14}N from the proximal His in the hhMbCN and the *Ma*Pgb*F-(G8)145WCN case, and thus do not point to a significantly increased His-Fe(III) bond strength in the latter protein. Theoretical computations have also linked the heme distortions to potential modulation of the oxygen affinity in ferrous globins such as protoglobins.[31]

We here also observe that mutation of the Phe(G8)145 residue, situated in ligand tunnel 1 in the vicinity of the heme group (Figure 1a), induces marked changes in the *g* values of the cyanide-ligated form. This gives experimental support to the recent theoretical prediction that the Phe(G8)145 residue plays an important role in ligand binding modulation and is involved in functional ligand recognition.[11] Furthermore, removal of the N-terminal 20 amino-acids, shown to be held next to the heme propionate groups in the crystal structure of *Ma*Pgb*O_2, also induces changes in the EPR spectrum of the corresponding cyanide-ligated protein, indicating that the N-terminal 20 amino-acid loop indeed affects the heme pocket.

■ ASSOCIATED CONTENT

Supporting Information

This information includes (1) figure showing the stabilization of the heme by the N-terminal loop, (2) estimation of the upper value of g_x from pulsed EPR; (3) comparison of the heme distortions of hhMbCN and MaPgb*O_2; (4) Comparison between simulated and experimental HYSCORE spectra; (5) ^{1}H Mims ENDOR spectra; (6) ligand-field analysis. This material is available free of charge via the Internet at http://pubs.acs.org.

■ AUTHOR INFORMATION

Corresponding Author

*Phone: +32 3 265 24 61. Fax: +32 3 265 24 70. E-mail: sabine.vandoorslaer@ua.ac.be.

Notes

The authors declare no competing financial interest.

■ ACKNOWLEDGMENTS

S.V.D., L.M., and S.D. acknowledge the Fund for Scientific Research Flanders (FWO) for funding (Grant G.0247.09). S.V.D. thanks support from the Hercules Foundation, Flanders (contract AUHA013).

■ REFERENCES

(1) Vinogradov, S. N.; Moens, L. *J. Biol. Chem.* **2008**, *283*, 8773−8777.

(2) Hou, S.; Freitas, T.; Larsen, R. W.; Piatibratov, M.; Sivozhelezov, V.; Yamamoto, A.; Meleshkevitch, E. A.; Zimmer, M.; Ordal, G. W.; Alam, M. *Proc. Natl. Acad. Sci. U.S.A.* **2001**, *98*, 9353−9358.

(3) Freitas, T. A. K.; Hou, S.; Dioum, E. M.; Saito, J. A.; Newhouse, J.; Gonzalez, G.; Gilles-Gonzalez, M. A. *Proc. Natl. Acad. Sci. U.S.A.* **2004**, *101*, 6675−6680.

(4) Vinogradov, S. N.; Hoogewijs, D.; Bailly, X.; Arredondo-Peter, R.; Gough, J.; Dewilde, S.; Moens, L.; Vanfleteren, J. R. *BMC Evol. Biol.* **2006**, *6*, 31.

(5) Vinogradov, S. N.; Hoogewijs, D.; Bailly, X.; Mizuguchi, K.; Dewilde, S.; Moens, L.; Vanfleteren, J. R. *Gene* **2007**, *398*, 132−142.

(6) Nardini, M.; Pesce, A.; Thijs, L.; Saito, J. A.; Dewilde, S.; Alam, M.; Ascenzi, P.; Coletta, M.; Ciaccio, C.; Moens, L.; Bolognesi, M. *EMBO Rep.* **2008**, *9*, 157−163.

(7) Pesce, A.; Tilleman, L.; Dewilde, S.; Ascenzi, P.; Coletta, M.; Ciaccio, C.; Bruno, S.; Moens, L.; Bolognesi, M.; Nardini, M. *IUBMB Life* **2011**, *63*, 287−294.

(8) Galagan, J. E.; Nusbaum, C.; Roy, A.; Endrizzi, M. G.; Macdonald, P.; FitzHugh, W.; Calvo, S.; Engels, R.; Smirnov, S.; Atnoor, D.; Brown, A.; Allen, N.; Naylor, J.; Stange-Thomann, N.; DeArellano, K.; Johnson, R.; Linton, L.; McEwan, P.; McKernan, K.; Talamas, J.; Tirrell, A.; Ye, W.; Zimmer, A.; Barber, R. D.; Cann, I.; Graham, D. E.; Grahame, D. A.; Guss, A. M.; Hedderich, R.; Ingram-Smith, C.; Kuettner, H. C.; Krzycki, J. A.; Leigh, J. A.; Li, W.; Liu, J.; Mukhopadhyay, B.; Reeve, J. N.; Smith, K.; Springer, T. A.; Umayam, L. A.; White, O.; White, R. H.; de Macario, E. C.; Ferry, J. G.; Jarrell, K. F.; Jing, H.; Macario, A. J. L.; Paulsen, I.; Pritchett, M.; Sowers, K. R.; Swanson, R. V.; Zinder, S. H.; Lander, E.; Metcalf, W. W.; Birren, B. *Genome Res.* **2002**, *12*, 532−542.

(9) Bapteste, E.; Brochier, C.; Boucher, Y. *Archaea* **2005**, *1*, 353−363.

(10) Battistuzzi, F. U.; Feijao, A.; Hedges, S. B. *BMC Evol. Biol.* **2004**, *4*, 44.
(11) Forti, F.; Boechi, L.; Bikiel, D.; Martí, M. A.; Nardini, M.; Bolognesi, M.; Viappiani, C.; Estrin, D.; Luque, F. J. *J. Phys. Chem. B* **2011**, *115*, 13771−13780.
(12) Walker, F. A. *Coord. Chem. Rev.* **1999**, *185*−*186*, 471−534.
(13) Hori, H. *Biochem. Biophys. Acta* **1971**, *251*, 227−235.
(14) Mulks, C. F.; Scholes, C. P.; Dickinson, L. C.; Lapidot, A. *J. Am. Chem. Soc.* **1979**, *101*, 1645−1654.
(15) Ohba, Y. *Appl. Magn. Reson.* **2003**, *23*, 539−556.
(16) Magliozzo, R.; Peisach, J. *Biochemistry* **1993**, *32*, 8446−8456.
(17) Arcovito, A.; Benfatto, M.; Cianci, M.; Hasnain, S. S.; Nienhaus, K.; Nienhaus, G. U.; Savino, C.; Strange, R. W.; Vallone, B.; Della Longa, S. *Proc. Natl. Acad. Sci. U.S.A.* **2007**, *104*, 6211−6216.
(18) Bolognesi, M.; Rosano, C.; Losso, R.; Borassi, A.; Rissi, M.; Wittenberg, J. B.; Boffi, A.; Ascenzi, P. *Biophys. J.* **1999**, *77*, 1093−1099.
(19) Dewilde, S.; Kiger, L.; Burmester, T.; Hankeln, T.; Baudin-Creuza, V.; Marden, M. C.; Caubergs, R.; Moens, L. *J. Biol. Chem.* **2001**, *276*, 38949−38955.
(20) Stoll, S.; Schweiger, A. *J. Magn. Reson.* **2006**, *178*, 42−55.
(21) Höfer, P.; Grupp, A.; Nebenführ, H.; Mehring, M. *Chem. Phys. Lett.* **1986**, *132*, 279−282.
(22) Liesum, L.; Schweiger, A. *J. Chem. Phys.* **2001**, *114*, 9478−9488.
(23) Jeschke, G.; Rakhmatullin, R.; Schweiger, A. *J. Magn. Reson.* **1998**, *131*, 261−271.
(24) Mims, W. B. *Proc. R. Soc. London, Ser A* **1965**, *283*, 452−457.
(25) Davies, E. R. *Phys. Lett. A.* **1974**, *47*, 1−2.
(26) Ioanitescu, I. A.; Van Doorslaer, S.; Dewilde, S.; Moens, L. *Metallomics* **2009**, *1*, 256−264.
(27) Appleby, C. A.; Blumberg, W. E.; Peisach, J.; Wittenberg, B. A.; Wittenberg, J. B. *J. Biol. Chem.* **1976**, *251*, 6090−6096.
(28) Das, T. K.; Lee, H. C.; Duff, S. M. G.; Hill, R. D.; Peisach, J.; Rousseau, D. L.; Wittenberg, B. A.; Wittenberg, J. B. *J. Biol. Chem.* **1999**, *274*, 4207−4212.
(29) Ikeda-Saito, M.; Kimura, S. *Arch. Biochem. Biophys.* **1990**, *283*, 351−355.
(30) Yang, T.-C.; McNaughton, R. L.; Clay, M. D.; Jenney, F. E., Jr.; Krishnan, R.; Kurtz, D. M., Jr.; Adams, M. W. W.; Johnson, M. K.; Hoffmann, B. M. *J. Am. Chem. Soc.* **2006**, *128*, 16566−16578.
(31) Bikiel, D. E.; Forti, F.; Boechi, L.; Nardini, M.; Luque, F. J.; Martí, M. A.; Estrin, D. A. *J. Phys. Chem.* **2010**, *114*, 8536−8543.
(32) Olea, C.; Boon, E. M.; Pellicena, P.; Kuriyan, J.; Marletta, M. A. *ACS Chem. Biol.* **2008**, *3*, 703−710.
(33) Emerson, S. D.; La Mar, G. N. *Biochemistry* **1990**, *29*, 1556−1566.
(34) Peisach, J.; Blumber, W. E.; Wyluda, B. J. *Eur. Biophys. Congr. Proc.* **1971**, *1*, 109−112.
(35) Fittipaldi, M.; García-Rubio, I.; Trandafir, F.; Gromov, I.; Schweiger, A.; Bouwen, A.; Van Doorslaer, S. *J. Phys. Chem. B* **2008**, *112*, 3859−3870.
(36) Vinck, E.; Van Doorslaer, S.; Dewilde, S.; Mitrikas, G.; Schweiger, A.; Moens, L. *J. Biol. Inorg. Chem.* **2006**, *11*, 467−475.
(37) Scholes, C. P.; Van Camp, H. L. *Biochim. Biophys. Acta* **1976**, *434*, 290−296.
(38) Can, M.; Zoppellaro, G.; Andersson, K. K.; Bren, K. L. *Inorg. Chem.* **2011**, *50*, 12018−12024.
(39) Ikeue, T.; Ohgo, Y.; Saitoh, T.; Yamaguchi, T.; Nakamura, M. *Inorg. Chem.* **2001**, *40*, 3423−3434.
(40) Walker, F. A. *Inorg. Chem.* **2003**, *42*, 4526−4544.
(41) Yatsunyk, L. A.; Shokhirev, N. V.; Walker, F. A. *Inorg. Chem.* **2005**, *44*, 2848−2866.
(42) Ikezaki, A.; Nakamura, M. *Inorg. Chem.* **2002**, *41*, 2761−2768.
(43) Watson, C. T.; Cai, S.; Shokhirev, N. V.; Walker, F. A. *Inorg. Chem.* **2005**, *44*, 7468−7484.
(44) Taylor, C. P. S. *Biochim. Biophys. Acta* **1977**, *491*, 137−149.
(45) Alonso, P. J.; Martínez, J. I.; García-Rubio, I. *Coord. Chem. Rev.* **2007**, *251*, 12−24.
(46) McGarvey, B. R. *Coord. Chem. Rev.* **1998**, *170*, 75−92.
(47) McGarvey, B. R. *Quim. Nova* **1998**, *21*, 206−213.
(48) Astashkin, A. V.; Raitsimring, A. M.; Kennedy, A. R.; Shokhireva, T. Kh.; Walker, F. A. *J. Phys. Chem. A* **2002**, *106*, 74−82.
(49) Raitsimring, A. M.; Borbat, P.; Shokhireva, T. Kh.; Walker, F. A. *J. Phys. Chem.* **1996**, *100*, 5235−5244.
(50) Liptak, M. D.; Wen, X.; Bren, K. L. *J. Am. Chem. Soc.* **2010**, *132*, 9753−9763.
(51) Desmet, F.; Thijs, L.; El Mkami, H.; Dewilde, S.; Moens, L.; Smith, G.; Van Doorslaer, S. *J. Inorg. Biol. Biochem.* **2010**, *104*, 1022−1028.
(52) Scholes, C. P.; Falkowski, K. M.; Chen, S.; Bank, J. *J. Am. Chem. Soc.* **1985**, *108*, 1660−1671.
(53) Fahnenschmidt, M.; Bittl, R.; Rau, H. K.; Haehnel, W.; Lubitz, W. *Chem. Phys. Lett.* **2000**, *323*, 329−339.
(54) Safo, M. K.; Walker, F. A.; Raitsimring, A. M.; Walters, W. P.; Dolata, D. P.; Debrunner, P. G.; Scheidt, W. R. *J. Am. Chem. Soc.* **1994**, *116*, 7760−7770.
(55) Shokhireva, T. K.; Weichsel, A.; Smith, K. M.; Berry, R. E.; Shokhirev, N. V.; Balfour, C. A.; Zhang, H.; Montfort, W. R.; Walker, F. A. *Inorg. Chem.* **2007**, *46*, 2041−2056.
(56) Roberts, S. A.; Weichsel, A.; Qiu, Y.; Shelnutt, J. A.; Walker, F. A.; Montfort, W. R. *Biochemistry* **2001**, *40*, 11327−11337.
(57) Shokhireva, T. K.; Berry, R. E.; Zhang, H.; Shokhirev, N. V.; Walker, F. A. *J. Inorg. Biochem.* **2011**, *105*, 1238−1257.
(58) Neya, S.; Suzuki, M.; Hoshino, T.; Ode, H.; Imai, K.; Komatsu, T.; Ikezaki, A.; Nakamura, M.; Furutani, Y.; Kandori, H. *Biochemistry* **2010**, *49*, 5642−5650.